

PERIODIC CRACK-MODEL OF COMB TRANSDUCERS: EFFICIENCY AND OPTIMIZATION

E. DANICKI

Polish Academy of Sciences
Institute of Fundamental Technological Research
(00-049 Warszawa, Świątokrzyska 21, Poland)
e-mail: edanicki@ippt.gov.pl

A model for a comb transducer is investigated in which the comb-sample interface is modeled by a periodic system of cracks. Leaky interface crack waves are generated by a normal incident shear bulk wave beam or by an equivalent excitation of the comb teeth at the interface. The generation efficiency is analyzed in systems where both the comb and the sample halfspaces are from the same material, steel or aluminium, for different teeth width and period, and for the case of solid contact between the two halfspaces between cracks; the other case of sliding contact is discussed briefly. Numerical results show that up to 25% of the incident power can be transformed into interface crack waves by a comb tooth. Optimal number of comb teeth is estimated, and the transducer frequency response is discussed. Approximated relationships are presented that may help designing a comb.

1. Introduction

A model of comb transducer analyzed below was introduced in two earlier papers [1, 2]. They present the analysis of the bulk wave scattering by periodic cracks at the interface of two contacting elastic halfspaces (Appendix A). It has been shown that an interface “crack wave” can be excited by a normal incident bulk wave beam and that this is a leaky wave that sheds its energy back to bulk waves due to the interaction with periodic cracks.

In this paper we continue investigation of the crack wave generation using the convenient transfer function model developed in [2] (and shortly presented in Appendix B), that is applying indirect characterization of the incident bulk wave by certain equivalent excitation of comb teeth at the interface ($\hat{\mathbf{u}}_0$). This approach simplifies much the analysis and delivers sufficiently “flexible” tool for evaluation and optimization of the comb transducer parameters. For simplicity reasons, the same material is assumed for both the comb and the sample to which the comb is applied with solid contact between cracks. The incident wave is a normal propagating shear wave, characterized by a shear force at the comb teeth-sample contact area. (It is worth to note that in the considered

case, the normal stress at the interface vanishes [1] because both the contacting half-spaces vibrate accordingly in this direction. Thus the ‘solid contact’ means vanishing normal stress at the interface between two identical halfspaces. In the complementary case of sliding contact and vanishing shear stress, where the normal stress is applied at the interface, the resulting normal particle displacements of both halfspaces may overlap; this case requires cautious discussion, perhaps including nonlinear effects [3] which may prevent such transducer application in nonlinear investigation of materials [4]. This case is discussed only briefly at the end of this paper.)

The above mentioned relationship is

$$\bar{\mathbf{T}}_m = \mathbf{Y}_{m-n} \dot{\mathbf{u}}_n, \quad (1)$$

where $\bar{\mathbf{T}}_m$ is the total force exerted by the m -th comb tooth (placed at $x = m\Lambda$ where $\Lambda = 2\pi/K$ is the teeth, or crack period) onto the sample, $\dot{\mathbf{u}}_n$ is the equivalent excitation of the n -th tooth at the interface which interpretation is presented in Fig. 3 of [2]. It is sufficient here to describe it as an equivalent difference of displacement velocity of the comb tooth and the sample that accounts for the displacement velocity of the incident wave $\dot{\mathbf{u}}^I$. As concern \mathbf{Y} , its most important component discussed in this paper is that resulting from the propagation of crack waves along the interface and causing some distant teeth to respond to the excitation. In the considered case and the interface normal to y axis, $\dot{\mathbf{u}} = [\Delta\dot{u}_x, 0]$, $\bar{\mathbf{T}} = [\bar{T}_{yx}, 0]$, and \mathbf{Y} are all scalars.

We neglect the local bulk wave field around the excited tooth that vanishes much faster with distance $(n - m)\Lambda$ than the leaky interface crack waves do. The discussed part of the transfer function results from the residuum (at poles $\pm r_c$) of the discrete inverse Fourier transform integral presented below after [2]

$$\mathbf{Y}_k = \frac{1}{K} \int_{-K}^K \left(\frac{a}{r - r_c} + \frac{a}{r + r_c} \right) e^{-jrk\Lambda} \sin \pi \frac{r}{K} dr. \quad (2)$$

Note that in the considered systems ($|r_c| \approx 0$ with respect to K) the integration path can be extended to $\pm\infty$ within accepted accuracy and using the Cauchy theorem, the integral can be easily evaluated by residua (the Jordan’s lemma is satisfied).

Equation (1) allows us to evaluate 1) the delivered power from the excitation source $\dot{\mathbf{u}}_n$ directly to the crack interface waves, that is necessary in evaluation of the efficiency of the comb transducers, 2) how this efficiency depends on the comb/sample material, teeth width and period, 3) and how much power of interface wave can be achieved at the comb edge for long combs having many teeth, accounting for that some distant teeth contribute weakly due to the leaky nature of the interface crack waves causing them to decay along the propagation path. The above subjects are discussed details in this paper on the basis of extended numerical examples for steel and aluminium materials. The analysis is carried out for particular frequency (we apply $\omega = 10^6 \text{ s}^{-1}$ like in [1]), note however that varying K is equivalent to varying ω^{-1} at constant Λ as discussed in [1]. That means that the comb frequency characteristic can be figured out from the transducer efficiency dependence on K .

2. Approximation parameters

It is shown in [1] that the interface “free vibration” exists for certain wave number of cracks K_c , and the leaky interface crack waves exist for $K > K_c$. Thus the primary task is to find K_c for the considered system: crack width $2w$, the material of comb and sample (in this paper they are the same), and the type of contact between cracks (considered solid here). Figure 1 presents the results of computations carried out on the basis of theory presented in [1]. Note that the free vibrations correspond to $r_c = 0$ in Eq. (2), and that $a = 0$ in this case because, as was shown in [1], no normal incident bulk wave is able to excite them.

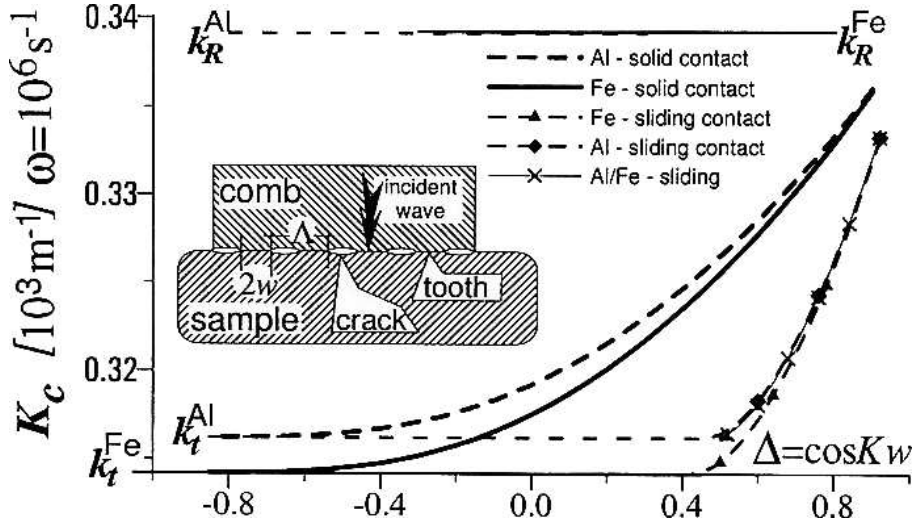


Fig. 1. “Free interface vibration” wave number K_c for cracks in steel (thick solid line) and aluminium (dash), for different crack width ($\Delta = \cos K_c w$). Thin lines with corresponding symbols present cases of sliding contact between the same or different halfspaces. Free vibrations, if exist, have their wave number between corresponding shear and Rayleigh wave numbers, k_t and k_R .

In Eq. (2), two parameters are introduced which must be evaluated numerically for the considered systems: the interface excitation strength a and the wave number r_c that is related to the wave number of the right propagating interface wave by $k_c = -r_c + K$. We apply r_c because conveniently $r_c^R = \text{Re}\{r_c\} > 0$ and $r_c^I = \text{Im}\{r_c\} > 0$. Naturally, $\text{Im}\{k_c\} < 0$ because the leaky wave propagating right, $\exp(j\omega t - jk_c x)$, decays at $x \rightarrow +\infty$ [2].

Starting from K_c , any higher K produces a and r_c different from 0, their evaluation is discussed in [2]. The results are presented in Fig. 2 for steel and aluminium, for several values of crack relative width characterized by $\Delta = \cos K w$ and for certain domain of $K > K_c$. The applied material data are for Al: $\rho = 2.7[10^3 \text{ kg/m}^3]$, $\mu = 27[10^9 \text{ Nm}^{-2}]$, $\lambda = 108[10^9 \text{ Nm}^{-2}]$ resulting in the shear wave number $k_t = .3162[1/\text{mm}]$, and for Fe: $\rho = 7.8$, $\mu = 79$, $\lambda = 112$, and $k_t = .3142$, in corresponding units.

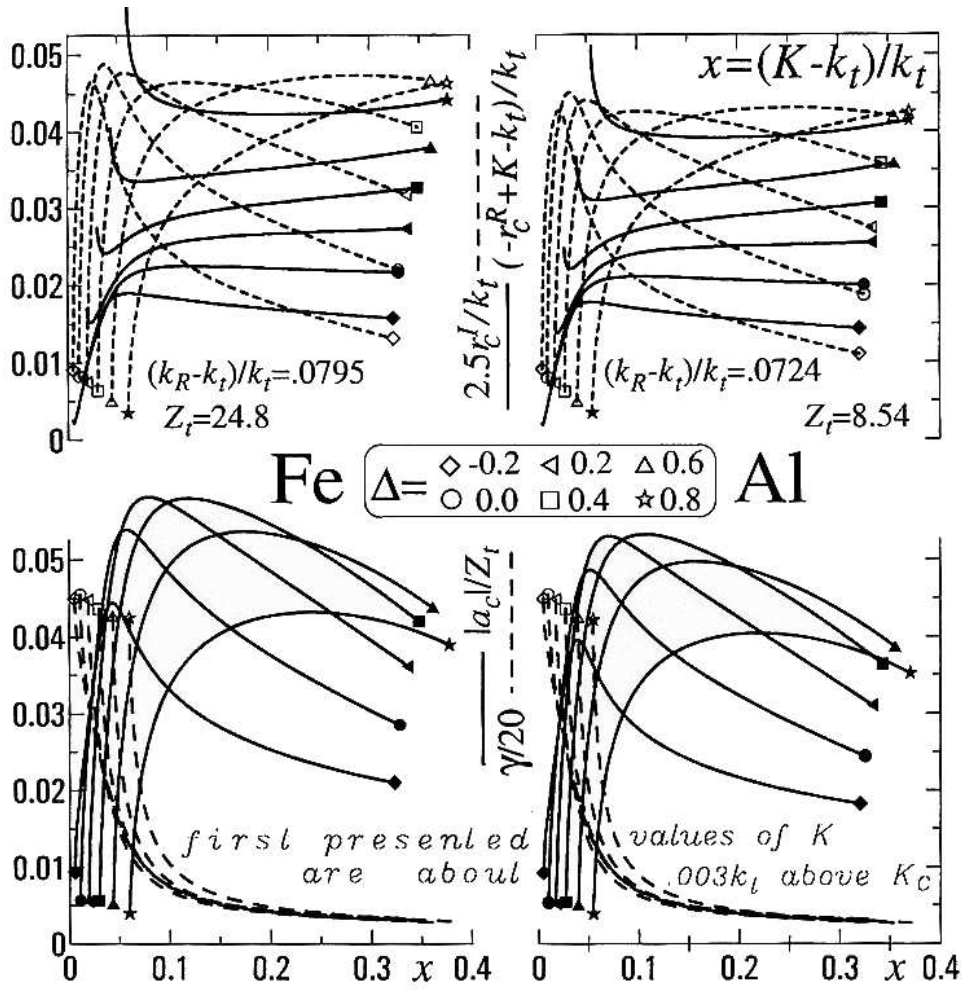


Fig. 2. Parameters of the spectral transfer function approximation, r_c and $|a_c|$, dependent on crack wave number K , for steel and aluminium and different Δ . Horizontal and vertical axes are nondimensional: $(k_c^* - k_t)/k_t$ (imaginary part of k_c^* is $2.5\times$ exaggerated) in the upper row, and a_c/Z_t in the lower. The interface wave number $k_c^R = K - r_c^R$ is little above k_t and almost constant for larger K , while its damping coefficient, r_c^I , has maximum at K close to k_t . If the difference $k_c - k_t$ is larger, then the interface wave field decays faster in depth of the body and thus is more similar and matched to Rayleigh waves propagating at free sample surface. Dash lines present a standing wave coefficient γ (actually $\gamma/20$ to match the scale) discussed in the last section.

3. Energy flow

Let's assume that only $\dot{\mathbf{u}}_0 \neq 0$, and the remaining $\dot{\mathbf{u}}_n$ are all zero accordingly to the solid comb/sample contact condition without existence of any incident bulk wave there (it means, within the interpretation of [2], that we consider a narrow incident wave beam of width constrained to a single comb period). Using Eqs. (1), (2), we easily obtain for

$m \neq 0$ on both sides of the excited tooth at $x = 0$

$$\overline{\mathbf{T}}_m = j\dot{\mathbf{u}}_0 \Lambda a_c e^{-jk_c |m|\Lambda}, \quad a_c = a \sin \pi r_c / K. \quad (3)$$

Neglecting unimportant phase, the total force exerted by m -th comb tooth on the contacting sample behaves like $|\overline{\mathbf{T}}_0| \exp(-r_c^I m \Lambda)$ where $\overline{\mathbf{T}}_0$ is a limit of $\overline{\mathbf{T}}_m$ as formally evaluated from Eq. (3) at $m \rightarrow 0$. This comb tooth/sample contact force results from the decaying leaky interface crack waves that spread the acoustic signal along the interface from the excited tooth to infinity in both directions. This was illustrated in figures presented in [2] in logarithmic scale producing easily recognizable linear dependencies with slope determined by r_c^I .

The above results deserves deeper discussion. For $r_c \sim 0$, the bulk wave reradiated due to the above mentioned leakage, propagates in almost normal direction to the interface. Moreover, the decaying is not very rapid so that we can consider this reradiated wave to be a planar wave, with different amplitude in different Λ -wide domains centered at $m\Lambda$. We know the total force in that domain, it is $|\overline{\mathbf{T}}_m|$, thus we may guess that the average stress in this Λ -wide domain is $\mathbf{T}_0 = |\overline{\mathbf{T}}_m|/\Lambda$. This average is the 0-th Bloch component of the interface stress distribution discussed detailedly in [1].

The surface stress \mathbf{T}_0 (this is a shear stress in the discussed system) excites shear bulk waves of power density $\Pi_y = |\mathbf{T}_0|^2/Z_t$ combined in both upper and lower halfspaces, where $Z_t = \sqrt{\rho\mu}$ is the acoustic impedance. (Exact evaluation of the wave field components and powers is presented in Appendix C.) The power reradiated into bulk in one Λ -wide domain is $\Lambda \Pi_y$ (the power per comb tooth), and the total reradiated (“leaking”) power on both sides of the excited tooth is

$$P^{\text{lk}} = \frac{2}{Z_t \Lambda} \sum_{m=1}^{\infty} |\overline{\mathbf{T}}_0|^2 e^{-2r_c^I m \Lambda}, \quad (4)$$

that must be equal to the total power of the generated interface waves in both directions, that is $2\Pi^c$ where Π^c is the right-propagating interface wave power.

Thus, on the strength of Eqs. (3), (4), we obtain important estimation

$$\Pi^c = \frac{1}{2r_c^I Z_t} \left| \frac{\overline{\mathbf{T}}_0}{\Lambda} \right|^2 = \frac{1}{2} \frac{|a_c|^2}{r_c^I Z_t} |\dot{\mathbf{u}}_0|^2, \quad (5)$$

for the crack wave power generated in one direction by a single tooth. It depends on the excitation strength $\dot{\mathbf{u}}_0$, and also on both spectral transfer function parameters discussed in previous section: r_c and a . (We apply notation of Π for the power flux density: $[\text{Wm}^{-2}]$ for bulk waves and $[\text{Wm}^{-1}]$ for interface waves, and P for total delivered power: Π multiplied by a beam width of bulk waves, for instance.)

In general, the parameter a in Eqs. (2), (3) has complex value. It describes the complicated phenomenon of crack wave generation by the excited comb tooth in presence of the bulk wave field that is excited simultaneously, and which field is described by the term const in Eq. (20) of [2]. This term is neglected in Eq. (2) of this paper; only terms describing interface waves alone are accounted for there. The resulting simplified approximation cannot be used for evaluation of the delivered power to the system through 1) evaluation

of the resulting force at the excited tooth $\overline{\mathbf{T}}_0$, and 2) applying it in the relation for the executed work $.5\text{Re}\{\overline{\mathbf{T}}_0\dot{\mathbf{u}}_0^*\}$, because $\overline{\mathbf{T}}_0$ is not the full force there.

There is another point of view however, by analogy to the similar problem for interdigital transducers [5]. We can apply another parameter a' in Eq. (2) instead of the original complex a , in order to evaluate the work on excitation of the *isolated* interface waves only, provided that 1) a' has imaginary value so that the power delivered to the system by far spectrum ($|r|$ large) vanishes (and vanishes if there are no poles at all), and 2) the excited wave field, in our case $|\overline{\mathbf{T}}_m|$, evaluated with a' is the same as that evaluated with a .

Both conditions are immediately satisfied by applying $a' = j|a|$. This makes the relation (2) to describe correctly the system supporting the isolated crack waves only, thus the evaluated force under the excited tooth can be used for evaluation of the executed power on *excitation* of interface waves, that is, the power delivered to crack waves alone

$$\overline{\mathbf{T}}_0' = \frac{\dot{\mathbf{u}}_0}{2K} \int_{-\infty}^{\infty} \left(\frac{|a|}{r - r_c} + \frac{|a|}{r + r_c} \right) (e^{jr\Lambda/2} - e^{-jr\Lambda/2}) dr. \quad (6)$$

Note that the Jordan lemma is satisfied either in lower or upper complex halfspaces of r . This yields $\overline{\mathbf{T}}_0' = j\Lambda|a|\exp(jr_c\Lambda/2)$, and finally the delivered power to the system

$$P^{\text{div}} = \frac{1}{2}\text{Re}\{\overline{\mathbf{T}}_0'\dot{\mathbf{u}}_0\} = \frac{1}{2}|\dot{\mathbf{u}}_0|^2|a|e^{-r_c\Lambda/2}\sin\pi r_c^R/K, \quad (7)$$

which power must be equal to the earlier evaluated total power of both excited crack waves. This produces the relationship that is fairly well satisfied in the computed examples

$$|a| = Z_t r_c^I r_c^R |r_c|^{-2}. \quad (8)$$

Direct evaluation of the excited crack wave power that verifies the above estimation is presented in Appendices C and D; that evaluation is used primarily in the computed results presented below.

4. Transducer efficiency

It results from Eq. (22) of [2] that the incident wave of particle displacement velocity $\dot{\mathbf{u}}^I$ is modelled by $\dot{\mathbf{u}}_0 = 2\dot{\mathbf{u}}^I$ in Eq. (1). Using again the plane wave approximation to the incident shear wave beam of one period width, the estimated incident power is $P^I = .5\Lambda|\dot{\mathbf{u}}_0/2|^2/Z_t$. The one-sided generation efficiency of a single comb tooth (accounting for only the interface wave propagating in either right or left direction), can be defined as

$$\eta_1 = P^c/P^I = r_c^R \Lambda \frac{r_c^I r_c^R}{|r_c|^2}, \quad (9)$$

where we exploited Eqs. (7) and (8). This strikingly simple estimation is valid for close to normal incidence and small r_c , independently of the teeth width or period, but may be less accurate for larger values of $K - K_c$. The bulk to crack wave conversion coefficient is

twice that: $2\eta_1 \approx r_c^R A \text{Im} \{(r_c/|r_c|)^2\}$. Figure 3 presents the single comb tooth efficiency evaluated for aluminium and steel materials. Up to about 25% of the incident wave beam power can be transformed into the interface waves by a tooth in both left and right directions (Appendix E). This is equivalent to about 5% of the incident power in an interface wave in the sample alone and in one propagation direction.

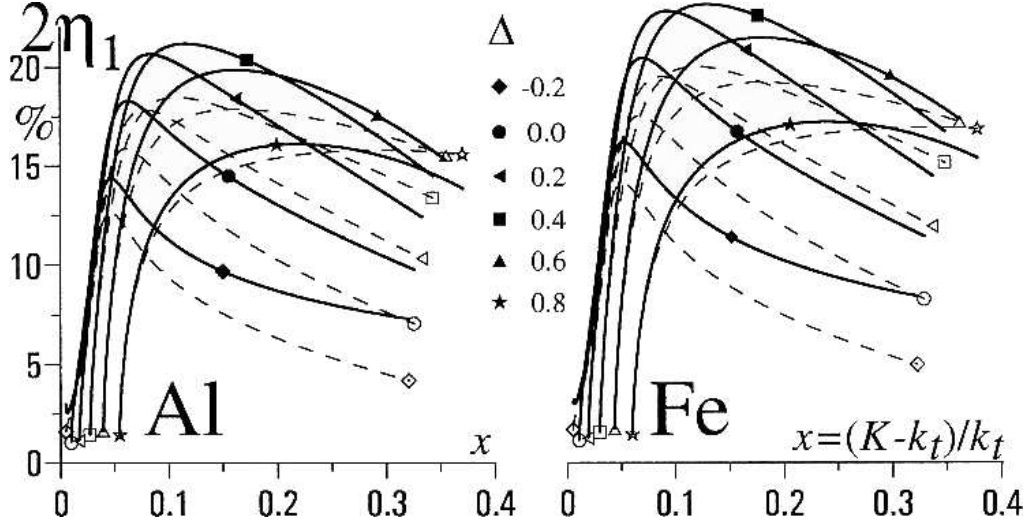


Fig. 3. A single tooth efficiency for aluminium and steel, for normal incident shear wave and solid contact between cracks, evaluated with help of Appendices A and B. Dash lines present the estimated values, Eq. (9). Maximum efficiency is achieved with comb teeth $\sim 30\%$ narrower than half teeth period ($\Delta \sim 0.4$).

It is interesting how much power can be transformed into an interfacial wave by direct tooth excitation, that is by applying $\dot{\mathbf{u}}_0$ neglecting how that can be done practically. This depends on how much bulk wave power is simultaneously generated by $\dot{\mathbf{u}}_0$. This depends on the neglected const in the approximation (2) to $\mathbf{Y}(r)$, see Eq. (20) of [2]. This const can be evaluated by applying small value of $r \ll r_c^R$ in Eq. (17) of [2]. The resulting Fig. 4 shows that this const = 0 for certain K_o . In this case the bulk wave radiation ceases; only interface waves are generated in both directions from the excited tooth. If there are many excited teeth, the evaluated interface wave field looks like these presented in Fig. 4. This figure computed using FFT like in the paper [2] shows that indeed at K_o , the interface wave field includes only the decaying crack waves, without bulk waves.

From practical point of view, more important is the maximum interface wave power that can be generated for given uniform excitation. Each of comb teeth contributes to the crack wave power. For $M = 2N - 1$ excited teeth, the resulting interface wave amplitude can be characterized by a force of the next to the last excited tooth in the system

$$|\bar{\mathbf{T}}_N| = \left| \dot{\mathbf{u}}_0 \sum_{l=1-N}^{N-1} \mathbf{Y}_{N-l} \right| \approx |\dot{\mathbf{u}}_0| \frac{A}{2} |a| |1 - e^{j r_c M \Lambda}|, \quad (10)$$

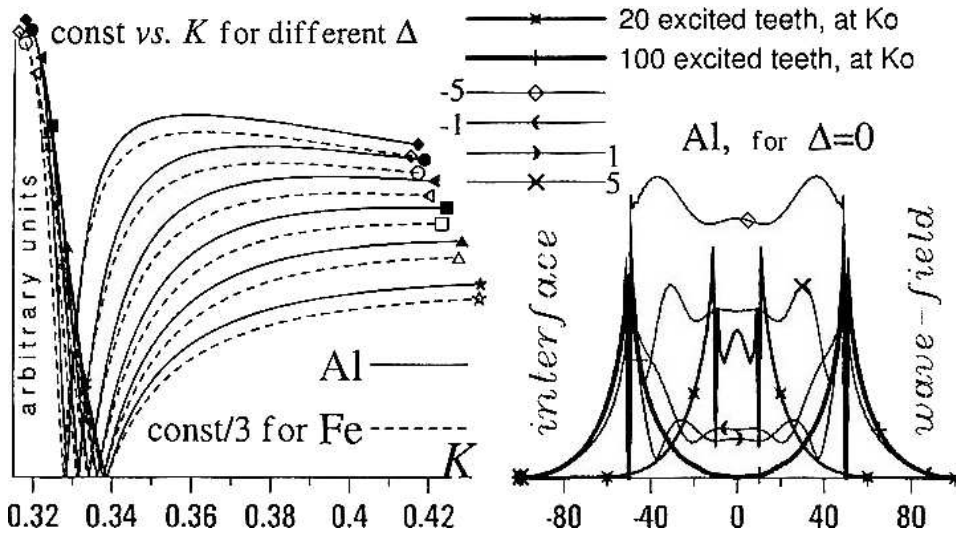


Fig. 4. The const part of $Y(r)$ that is responsible for direct bulk wave generation by the excited comb teeth, vanishes at certain K_0 . The wave-field exponential shape inside the uniform excitation domain of 100 teeth confirms well that there is almost exclusively an interface wave without a floor of bulk waves. This is not the case if $K \neq K_0$, shown here for comparison. This figure clearly shows that applying more teeth than optimal does not produce any higher interface wave amplitude: compare wave-fields outside the excitation domains of 20 and 100 teeth.

Its value is $|1 - e^{jr_c M \Lambda}| |2 \sin \pi r_c / K|^{-1}$ times greater from the earlier evaluated $|\bar{T}_1|$ for a single excited tooth, Eq. (3).

Applying this value for estimation of the crack wave power, Eq. (5) or the corresponding relations from Appendix C, we obtain that

$$\Pi^c = \Pi_\infty |1 - e^{jr_c M \Lambda}|^2, \quad \Pi_\infty = \frac{P^I}{2r_c^I \Lambda} |a/Z_t|^2, \quad (11)$$

where $P^I = .5Z_t \Lambda |\dot{u}^I|^2$ is the incident power per comb period. In the limit of infinite comb, $\Pi^c = \Pi_\infty$. The coefficient $g = \Pi^c / P^I$ shows how much times the crack wave power is greater than the incident bulk wave power per comb period. The transformation efficiency of comb transducer is g/M because the total incident power is MP^I . Example dependences of the generated interface wave power on a number of exciting comb teeth are shown in Fig. 5 (reminding the correspondence of ω and K^{-1} , this figure also represents the comb frequency response). There are local maxima resulting from certain interference of contributions of the edge comb teeth that ceases with growing M because of wave damping, $r_c^I > 0$. For given K , the first maximum appears at M where

$$e^{-r_c^I M \Lambda} \sin \phi = \sin(r_c^R M \Lambda + \phi), \quad \sin \phi = r_c^I / |r_c| \quad (12)$$

$(\pi - 2\phi < r_c^R M \Lambda < \pi - \phi)$. This M is an optimal number of teeth making the comb to produce the maximum power of an interface crack wave.

It depends on r_c how many teeth the comb must count to achieve the maximum crack wave power. In practice, the comb should have number of teeth evaluated for K produc-

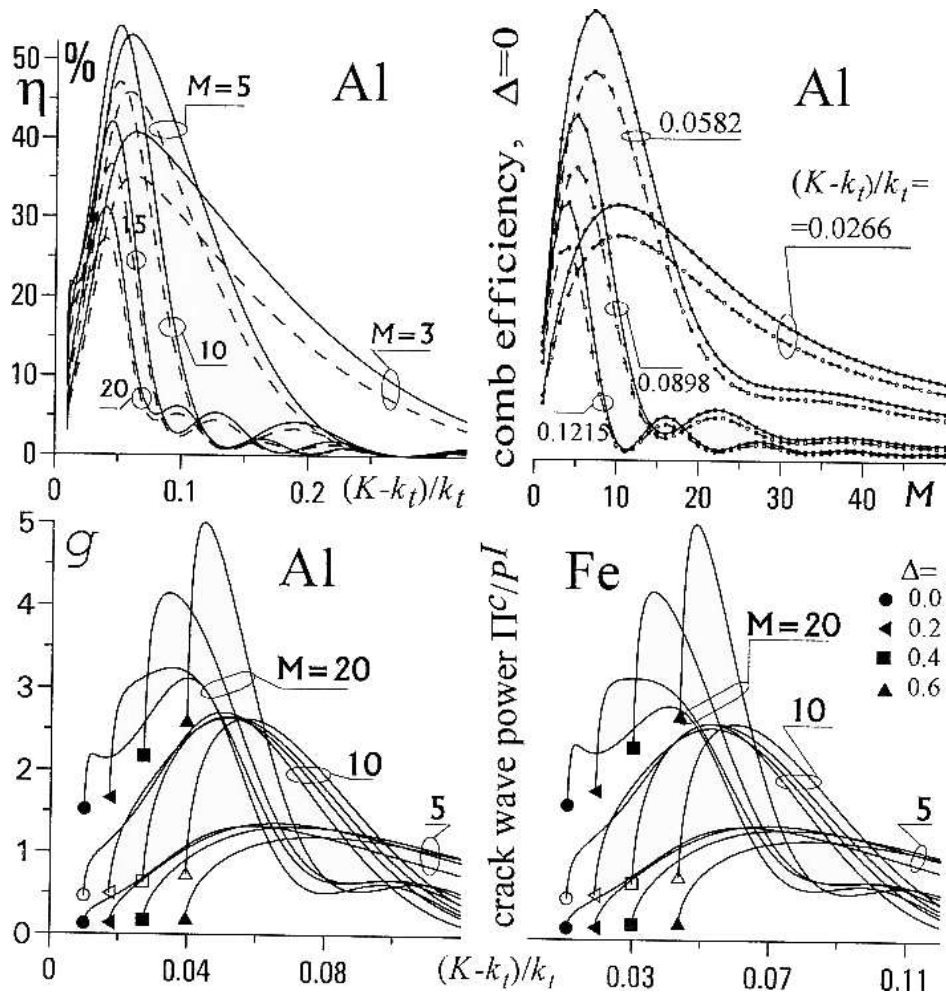


Fig. 5. Power conversion efficiency of combs with different teeth number M , as evaluated from the crack wave power (solid lines) and estimated (dash lines). Accounting for that $\omega \sim K^{-1}$ for given comb period, the frequency characteristic of comb can be figured out from the comb efficiency dependence on K . Figures show that, for reasonable values of M , the maximum efficiency is achieved at K not much higher from K_c , and that the efficiency is higher for narrower teeth, at cost of narrower passband, which relative width is generally smaller by half, than M^{-1} .

ing the highest interface crack power. Figure 6 presents the convenient dependency of maximum interface power on the optimal number of teeth, both evaluated for given K . This parametric dependence (with parameter K), is sufficient for the comb optimization: we seek the largest power possible within the required passband that is inversely proportional to the teeth number (Fig. 5).

In the discussed transfer function model, we neglected the term resulting from the unknown \mathbf{T}_0 in Eq. (B.1). Now we check the validity of this assumption. Figure 6 presents the interface wave field evaluated from the model and evaluated directly from

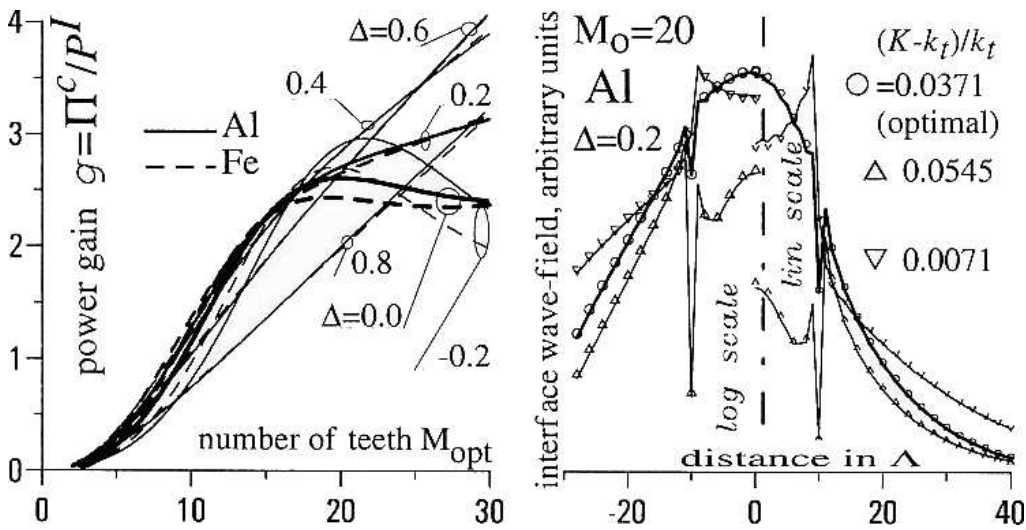


Fig. 6. A basis for comb optimization: the parametric dependence of maximum, with varying K , of the generated crack wave power on the teeth number M : for given K , an optimal M is evaluated and then the resulting crack wave power at the comb edge. Much higher power can be achieved with larger but not practical values of M resulting for lower K , and for narrower teeth width because of smaller crack wave leakage: smaller r_c^I at low $K - K_c$. Example interface wave-fields are shown for optimal value of $M_o = 20$ teeth assumed somewhat narrower than half period Λ ($\Delta = 0.2$), inside and outside the comb domain and for optimal, lower and higher values of K . They are evaluated using the model (lines), and by applying the “ $\sin x/x$ ” angular spectrum of incident wave beam $\mathbf{T}^I(r)$ in Eq. (A.1) (symbols). The overlapping results confirm the assumptions applied in modeling the teeth excitation (Appendix B).

Eqs. (A.1)–(A.5), by applying $\mathbf{T}^I(r) = M \sin(rM\Lambda/2)/\sin(r\Lambda/2)$: this is an approximated spectrum of uniform incident wave beam of width $M\Lambda$. The agreement is excellent.

5. A modified comb

Let’s consider a slightly oblique incidence, at angle α off normal. It results in the interface force having different phase at different comb teeth: $\dot{\mathbf{u}}_t = \dot{\mathbf{u}}_0 \exp(jl\Lambda k_t \sin \alpha)$. Neglecting the origin of these forces, whether resulting from an incident wave or from a direct teeth excitation, their spectral representation at the interface plane has the known “ $\sin x/x$ ” shape, $x = (r - k_t)M\Lambda/2$ where $M\Lambda$ is the excitation area.

For normal incidence considered in previous sections, this $\sin x/x$ function is centered at $r = 0$. The excited interface wave amplitude however, is evaluated from Eqs. (1), (2) at poles $\pm r_c \neq 0$. This means particularly that the interface waves are excited inefficiently by side, off-maximum spectral line of the excitation force, and can be near zero if r_c^R falls near zero of $\sin x/x$ (this depends on M). The remedy to this deficiency is discussed here. To place the maximum spectral line of the excitation force closer to r_c , we modify the comb transducer arrangement by applying oblique wave beam incidence. In order to stay within previously applied assumption of $T_{22} = 0$ at the comb/sample interface, two

oblique incident shear waves (with $\pm\alpha$ angle of incidence) should be generated by two piezoelectric slab transducers at the comb top. Their total normal power flux combined Π_y yields an equivalent teeth excitation $\dot{\mathbf{u}}_0 = \sqrt{2\Pi_y \cos \alpha / Z_t} \exp(\pm j k_I x)$ that is $\sqrt{\cos \alpha}$ times that of a single normal incident wave beam discussed earlier.

A pair of off-normal incident wave beams produces an interface excitation force having two spectral lines of $\sin x/x$ shapes with maxima placed at $\pm k_I$. We may assume that the left incident wave beam, producing spectral line at k_I , matches $r_c = K - k_c$ and produces only the left-propagating crack wave, and the right wave beam – the right interface wave only. For uniform excitation with variable phases, the amplitude of tooth force just right to the comb is

$$\begin{aligned} \bar{\mathbf{T}}_N &= \dot{\mathbf{u}}_0 \sum_l \int_{-K}^K \frac{a}{r + r_c} e^{j(r - k_I)(N-l)\Lambda} \sin \pi r / K \, dr / K, \\ |\bar{\mathbf{T}}_N| &\approx |a_c| |\dot{\mathbf{u}}_0| \Lambda \left| \frac{1 - \exp j(r_c - k_I)M\Lambda}{2 \sin(r_c - k_I)\Lambda/2} \right|, \end{aligned} \quad (13)$$

which $|\bar{\mathbf{T}}_N|$, like in all numerical results presented above, can be applied in equations of Appendices C, D in order to evaluate the interface power Π^c .

The maximum crack wave appears at $k_I = r_c^R$; this determines a center frequency of the structure. This maximum is $\sim M \exp(-r_c^I M \Lambda / 2)$ dependent on M , and there is optimal $M_o = 2/r_c^I \Lambda$ producing its largest value $\sim M_o/e$. The maximum value of $|\bar{\mathbf{T}}_N|/\Lambda$ is $|\dot{\mathbf{u}}_0| |a_c| M_o/e$ which value is used for the estimation of both generated interface waves power based on Eqs. (5) and (8).

$$2\Pi_{\max}^c \approx 8 \frac{\Pi_y \Lambda \cos \alpha}{r_c^I \Lambda} \left| a \frac{r_c \Lambda}{2Z_t} \right|^2 \frac{M_o}{e^2} \frac{2}{r_c^I \Lambda}, \quad (14)$$

it can be as high as $.5\Pi_y M_o \Lambda$. It results that almost 50% conversion can occur in an optimal case.

The structure is promising. Particularly, $r_c - k_I$ can have purely imaginary value at center frequency. Thus the maximum interface wave power is *independent* of how large the value of r_c^R is, allowing us to exploit the optimal case of large a and small r_c^I in the whole domain of K . With small r_c^I , we get large optimal wave beam width $M_o \Lambda$ that is large total incident power, and large part of it can be converted into crack waves at center frequency.

6. Incident longitudinal waves

The short discussion here concerns the case of normal incidence of longitudinal wave beam and sliding contact between cracks. The same materials are assumed for the comb and the sample. Therefore the interface stress $\mathbf{T} = [0, T_{yy}]$, particle displacements $\mathbf{u} = [0, u_y]$, acoustic impedance $Z_t = \sqrt{\rho(2\mu + \lambda)}$, and proper transfer function \mathbf{Y} should be applied in the theory that is otherwise similar to that presented above for incident shear wave. Here we present only numerical results in the domain of K where Eq. (8)

is satisfied with adequate accuracy. This means that the same physical interpretation of the results holds in both cases.

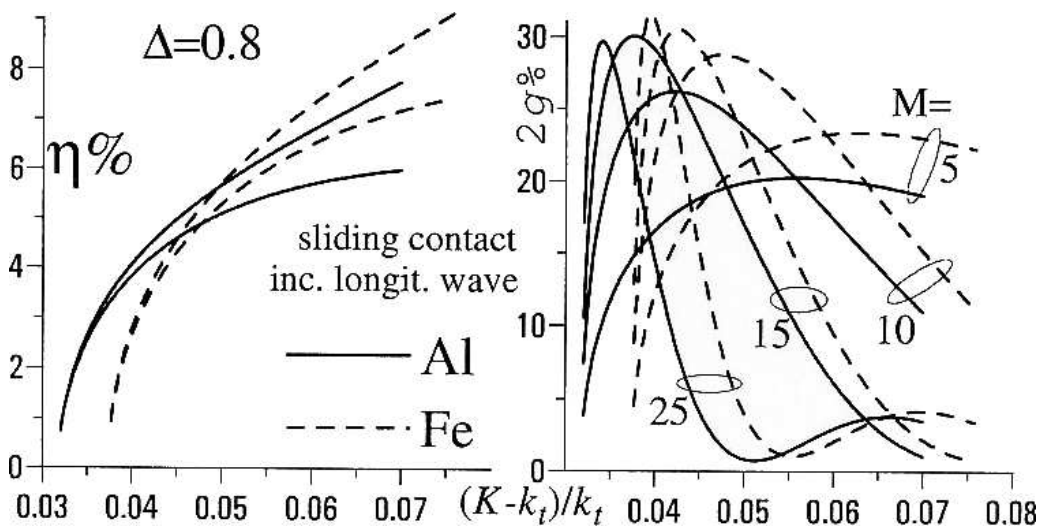


Fig. 7. Optimization figure for the case of incident longitudinal wave and sliding comb-sample contact. The efficiencies evaluated from the Bloch wave powers (higher values) and estimated, Eq.(9) (lower values), diverge at higher K indicating that the model loses its validity there. The comb efficiency is much lower than in the case of incident shear wave in the analogous domain of K and M .

We notice from Fig.1 that the free vibrations exist only for relatively wide crack and narrow teeth: below $\Lambda/3$ wide. Figure 7 presents the single tooth efficiencies, both evaluated from the energy flow of the generated wave-field, and from the approximation (8). Note that the efficiency is much lower than in the previously discussed case of solid contact in similar domain of K . This results in low efficiency of comb having practical $M < 25$ teeth; the generated power is much less than the incident power per comb period.

7. The edge phenomena

Above, we discussed the phenomenon of interface wave generation in infinite system of periodic cracks, that is the generation under an infinite comb attached to an infinite sample (albeit only finite number of teeth were insonified by the incident wave beam). The interface waves were assumed to propagate freely along the entire system. This assumption is correct for combs long enough with respect to the interface wave length $2\pi/k_c \approx \Lambda$, and is well satisfied for combs with near optimal number of teeth (10 or more, Fig. 6).

There is an edge however in any practical combs, where the crack waves can no longer propagate and thus the complicated phenomena of reflection, transformation into a Rayleigh wave existing outside comb, and scattering into bulk waves must be invoked.

It is far beyond the scope of this paper to cover adequately the resulting diffraction problem for semiinfinite periodic system (to focus attention on the single edge of a comb only). Instead, we will present a simplified model appropriate only for better physical understanding of comb transducers. We will consider only the wave field in the sample neglecting this part of the interface wave that propagating inside the comb, must fall on the comb walls and scatter. Moreover, we neglect the backward wave component of the interface waves.

The considered system is periodic, and thus the interface wave field is composed of series of Bloch components. Two of them, ± 1 st components carry energy along the interface: the 1st carries energy in positive direction with respect to the interface wave propagation, this is a forward propagating component, and the -1 st carries energy in opposite direction – this is a backward wave component. The power carried by an interface wave is the sum of both partial powers $\Pi^c = \Pi^{(1)} + \Pi^{(-1)}$, accounting for that $\Pi^{(-1)} < 0$. These two components may have quite different wave numbers: $k_c = k_1 = -r_c + K$ and $k_{-1} = -r_c - K$ respectively for the forward and backward components of a crack wave propagating right, and they decay quite differently in depth of the sample [1]. This makes the considered scattering phenomenon much more complicated than the corresponding phenomenon of interdigital transducers where both forward and backward components are only weakly perturbed Rayleigh modes [3] in which case the exploited simplification leads to the reflection/transmission problem only.

Examples of the standing wave coefficients $\gamma^2 = -\Pi^{(-1)}/\Pi^{(1)}$ in the considered structures are presented in Fig. 2, as yet another characterization of interface waves. We notice that $\gamma \rightarrow 1$ at $K \rightarrow K_c$; this explains why the interface “free vibrations” ($K = K_c$) do not transport energy along the interface: the energy carried back by backward Bloch component compensates perfectly the energy carried forward by the forward component. For greater K however, $\gamma < 1$ and the backward energy transport diminishes allowing some net energy to be transported along the interface; this is the interface wave power. In what follows, we will consider the case of small γ , allowing us to neglect the backward wave component. This simplifies the modeled wave scattering phenomenon. It is still however, much more complicated than that for interdigital transducers because of proximity of wave numbers k_c and k_t (the shear wave number). Due to the resulting significant difference in the penetration depths of crack and Rayleigh waves, much power is expected to be scattered into bulk waves.

Summarizing, the model of the scattering problem is the following. There is a semi-infinite comb where an interface wave propagates (only its forward propagating Bloch component is accounted for but its damping is neglected, $\text{Im}\{k_c\} \rightarrow 0$) towards the edge where it scatters producing the transmitted Rayleigh wave outside the comb, and also producing the reflected interface wave and bulk waves. We are interested mostly in the transmitted Rayleigh wave amplitude and also in the reflected interface wave because it can result in certain spurious “ringing” phenomenon in real finite combs. The problem is considered in detail in Appendix F with help of the Wiener-Hopf technique [6]. Figure 8 presents the computed examples. Generally, the interface wave to Rayleigh wave transformation depends strongly on k_c when $k_c \sim k_t$. In practical combs however, k_c does not change much with K (Figs. 2 and 3) and thus the transmission coefficient does not

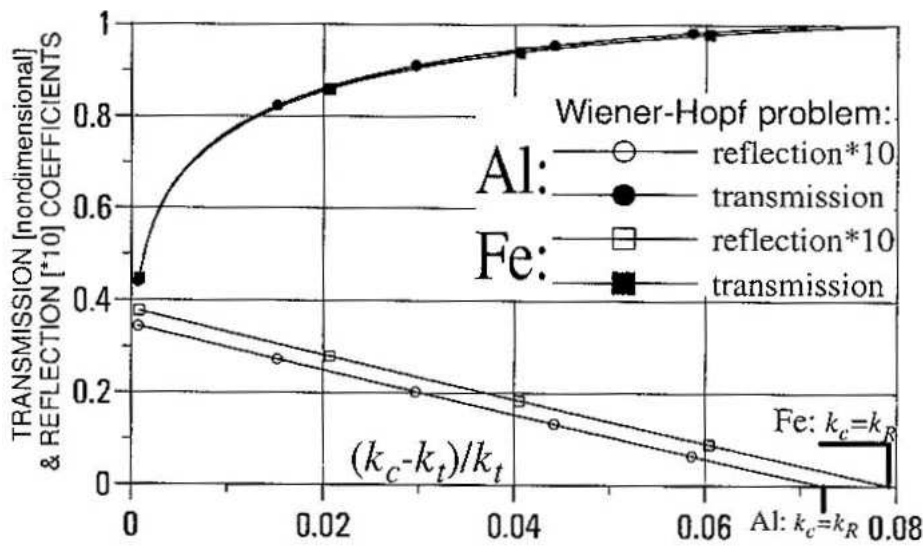


Fig. 8. An interface to Rayleigh wave transformation at the comb edge, estimated on the basis of the Wiener-Hopf diffraction problem: the incident and the reflected crack waves have wave numbers $\pm k_c$, the transmitted is the Rayleigh wave with wave number k_R . The transmission is low when k_c is close to k_t , and is full when $k_c \approx k_R$. Reflection coefficient is small, few percents, and can be neglected. The remaining part of the incident wave power is scattered into bulk waves.

change significantly with K : it is approximately 90%. The reflection coefficient can be neglected.

8. Conclusions

Comb transducers are rather complicated structures. The developed model is perhaps the simplest but powerful enough to figure out the transducer basic parameters: efficiency and frequency response, and can be used for certain optimization of the system. Moreover, the model reveals a number of wave phenomena involved in the bulk to Rayleigh wave transformation needed for better understanding the comb in practical use.

Summarizing the numerical results presented in this paper we conclude that the efficiency of comb transducers is not high; about 5% of the incident power (MP^I) is transformed into right-propagating Rayleigh wave in the sample only. The usefulness of comb relies however on using large P^I (incident power per comb period) to generate strong Rayleigh wave of power $\sim 2P^I$. The overall efficiency can be perhaps improved with the proposed modified comb (oblique incidence).

Surprisingly, the optimal number of comb teeth (~ 20) agree with practical applied combs [4] (they are usually glued to the sample with salol to make rather solid contact; practical comb teeth height is a fraction of comb period, and the crack model with infinitesimal teeth height seems acceptable). However, low expected efficiency of comb with longitudinal incident wave is rather disappointing.

Perhaps higher efficiency at smaller M and wider transducer passband can be achieved with different comb material of rather low acoustic impedance and especially optimized for given types of materials, e.g. steel or aluminium. Anisotropic or composite materials can also be analyzed within the developed technique.

Acknowledgments

Dr. Donna Hurley from NIST, Boulder, is acknowledged for sharing her experience with comb transducers, and also for her kind assistance in preparation of this paper. Financial support was provided by the Polish-US Maria Curie Skłodowska Joint Fund II under Grant No. PAN/NIST-97-300. This paper is dedicated to the memory of Maria Curie Skłodowska, a double Nobel laureate.

Appendix A: The scattering problem

An elastic halfspace $y > 0$ is characterized in spectral domain by a harmonic Green's relationship $\mathbf{u} = \mathbf{G}\mathbf{T}$, where \mathbf{u} and \mathbf{T} are surface particle displacement and stress; \mathbf{G} is the Green's matrix for the sample. The incident wave in comb material is characterized by $\mathbf{u}^I = \overline{\mathbf{G}}\mathbf{T}^I$. The scattering problem of bulk waves on cracks is described by a system of equations [1]

$$[\mathbf{g}_\infty S_{n-m} - \mathbf{g}(r + nK)]\mathbf{t}_m P_{n-m}(\Delta) = -\dot{\mathbf{g}}(r)\delta_{n0}\mathbf{T}^I(r), \quad (\text{A.1})$$

for n -th Bloch wave field component, $r \in (0, K)$. There is summation over $m \in [-N, N+1]$, P_ν is a Legendre function, and

$$\mathbf{g}(p) = -jp \left(\mathbf{G} + \overline{\mathbf{G}}^T \right), \quad \dot{\mathbf{g}}(p) = -jp \left(\overline{\mathbf{G}} + \overline{\mathbf{G}}^T \right). \quad (\text{A.2})$$

The applied method of solution allows us to constrain n to a finite domain: $n \in [-N, N]$, where $N \gg k_t/K$ (the domain of n is shifted left for $r \sim K$); we used $N = 3$ in computations.

The equation results from a contact condition between comb and sample

$$\overline{\mathbf{u}} = \frac{j\pi}{K \sin \pi r/K} \mathbf{g}_\infty (-1)^m \mathbf{t}_m P_{-m-r/K}(-\Delta) = 0 \quad (\text{A.3})$$

that closes the system.

Now, $\mathbf{t}_m(r)$ can be evaluated for any r and given spectrum of the incident wave $\mathbf{T}^I(r)$. For example, the n -th Bloch component of the interface stress is

$$\mathbf{T}_n = \mathbf{t}_m P_{n-m}(\Delta). \quad (\text{A.4})$$

and the spectral representation of a discrete interface force is

$$\overline{\mathbf{T}}(r) = \Lambda \mathbf{t}_m P_{-m-r/K}(\Delta), \quad (\text{A.5})$$

which inverse Fourier transform over domain $(0, K)$ yields $\overline{\mathbf{T}}_l$, the total force exerted by l -th comb tooth on the sample. This force may result directly from the incident wave

beam or, if l is outside the area of incidence $(-M/2, M/2)$, from the generated interface waves. In this case $\bar{\mathbf{T}}_{M/2+1}$ can be used for evaluation of the crack wave amplitude. This straightforward evaluation of the excited interface wave was applied in [2]. In this paper, we apply the transfer function model presented in Appendix B.

Appendix B: The model

Following the earlier development [2], the incident wave \mathbf{T}^I can be equivalently characterized by a direct teeth excitation $\dot{\mathbf{u}}$. Here, we present shortly how, and with what approximation, can this be done.

It is assumed here that r/K is small. This is reasonable if the normal incident wave beam is wide and thus its spectrum is narrow, see Eq. (A.1). In what follows, we will neglect small terms of an order of r . Noticing first that the right-hand side of the Eq. (A.1) at $n = 0$ is small ($\sim r$), we divide it by $-jr$ and add to Eq. (A.3) multiplied by $jK \sin(\pi r/K)/\pi \approx -jr$. This yields

$$-jr^{-1} \mathbf{g}_\infty [S_{-m} P_{-m}(\Delta) - (-1)^m P_{-m-r/K}(-\Delta)] \mathbf{t}_m = 2\mathbf{u}^I - [\mathbf{G} + \bar{\mathbf{G}}^T] \mathbf{T}_0, \quad (\text{B.1})$$

because $\dot{\mathbf{g}}\mathbf{T}^I = 2\mathbf{u}^I$. The other component on the right-hand side, $(\mathbf{G} + \bar{\mathbf{G}})\mathbf{T}^{(0)}$ is still unknown. We will have to check it *a posteriori* if this term can be neglected.

Note that the coefficients of above equation are of an order of r^0 , thus finite with $r \rightarrow 0$. Moreover, with the accepted accuracy, Eq. (A.1) at $n = 0$ becomes

$$\mathbf{g}_\infty S_{-m} \mathbf{t}_m P_{-m}(\Delta) = 0. \quad (\text{B.2})$$

It makes possible to neglect the first term of (B.1), and thus for $r \rightarrow 0$, the Eq. (A.1) and the above equations yield the following system that constitute the model

$$\begin{aligned} [\mathbf{g}_\infty S_{n-m} - \mathbf{g}(r+nK)] \mathbf{t}_m P_{n-m}(\Delta) &= 0, \\ j\omega \mathbf{g}_\infty (-1)^m \mathbf{t}_m P_{-m-r/K}(-\Delta) &= \dot{\mathbf{u}} \sin \pi r/K, \end{aligned} \quad (\text{B.3})$$

which $\dot{\mathbf{u}}(r) = 2\dot{\mathbf{u}}^I - j\omega(\mathbf{G} + \bar{\mathbf{G}})\mathbf{T}^{(0)}$. Using Eqs. (A.5) and (B.3), we evaluate the spectral transfer function $\mathbf{R}(r)$ involved in

$$\bar{\mathbf{T}}(r) = \mathbf{R}(r) \dot{\mathbf{u}} \sin \pi r/K, \quad \mathbf{R}(r) \approx \text{const} + \mathbf{Y}(r), \quad (\text{B.4})$$

as presented in [2]. Its inverse Fourier transform yields Eq. (1), neglecting the const term, unimportant for interface waves.

The unknown component in $\dot{\mathbf{u}}$ on the right-hand side of Eqs. (B.3) requires certain further interpretation. We attempt to replace the incident wave, the true source of interface waves, by certain *known* teeth excitation at the interface. This is like attempting to neglect the intrinsic impedance of an electric voltage source, replacing it by *known* voltage at the load port. Naturally, we need to correct this voltage *a posteriori*, accounting for the voltage drop due to the current flowing through the impedance.

Something similar, but more complicated is the case considered in this paper: the interface equivalent excitation $\dot{\mathbf{u}}$ depends on the unknown 0-order Bloch component of

the interface stress \mathbf{T}_0 . The same stress is responsible for the leakage of interface waves which is rather small, allowing the wave to propagate along the interface. This suggest that it can be indeed neglected.

Moreover it is worth to note here that the interface stress \mathbf{T}_1 is, in fact, responsible for resonant generation of the interface waves because both have the same wave number $-r_c + K = k_c$ (for right propagating waves). Thus we can define alternatively the equivalent $\dot{\mathbf{u}}$ that reproduces, at $r = -r_c = k_c - K$ and in a domain around it, the original \mathbf{T}_1 resulting from \mathbf{T}^I in Eq. (A.1).

To check the validity of the above introduced model, we may evaluate $\mathbf{Y}(r)$ and \mathbf{T}_1 in both cases, that is using 1) Eqs. (A.1) and (A.3) with \mathbf{T}^I given, and 2) Eqs. (B.3) with given *equivalent* $\dot{\mathbf{u}}$, solving these equations and evaluating the above mentioned functions of r . The numerical verification proves that the above mentioned equivalent characterization is very satisfactory in most important domain of spectral variable $|r - r_c| \leq |r_c|$, for any K discussed in this paper. In fact, this is also confirmed in Fig. 6. As such, it can be used for evaluation of both r_c and a , and the Eq. (1) can be indeed applied in our analysis of comb transducers.

Appendix C: Amplitudes and powers

Introducing notation for longitudinal and shear partial wave amplitudes F_l and F_t , it was shown in [1] that

$$\begin{bmatrix} \dot{u}_1 \\ \dot{u}_2 \end{bmatrix} = \frac{j}{\sqrt{\rho\omega}} \begin{bmatrix} p & -q_t \\ q_l & p \end{bmatrix} \begin{bmatrix} F_l \\ F_t \end{bmatrix}, \quad (\text{C.1})$$

which $F_{l,t}$ can be evaluated from stress $\mathbf{T} = [T_{21} \ T_{22}]^T$ at $y = 0$

$$\begin{bmatrix} F_l \\ F_t \end{bmatrix} = j \frac{\omega}{\mu} \frac{\sqrt{\rho\omega}}{D} \begin{bmatrix} 2pq_t & k_t^2 - 2p^2 \\ 2p^2 - k_t^2 & 2pq_l \end{bmatrix} \begin{bmatrix} T_{21} \\ T_{22} \end{bmatrix}, \quad (\text{C.2})$$

where p is the wave number $r + nK$ of n -th Bloch component of a wave field; $q_{l,t}$ are p -dependent wave numbers in depth of the body of corresponding partial waves, and

$$\Pi_2 = \text{Re} \{ q_l |F_l|^2 + q_t |F_t|^2 \} / 2 \quad (\text{C.3})$$

is the y -component of the Poynting vector. It can be used for evaluation of the power shed by the interface wave into bulk wave, particularly by its 0-order Bloch component, $p = -r_c$ for the right propagating interface wave.

To evaluate the x -component of Poynting vector, we need T_{11} . It must be evaluated from equations of motion of the body

$$T_{11,1} + T_{12,2} = -\rho\omega^2 u_1, \quad (\text{C.4})$$

which, using (A.1-2), yields $T_{11} = j\mu[(2q_l^2 - k_t^2)F_l + 2pq_t F_t]/(\omega\sqrt{\rho\omega})$ and thus

$$[T_{11} \ T_{12}] = \frac{j}{\sqrt{\rho\omega}} \frac{\mu}{\omega} [F_l \ F_t] \begin{bmatrix} 2q_l^2 - k_t^2 & -2pq_l \\ 2pq_t & 2q_t^2 - k_t^2 \end{bmatrix}. \quad (\text{C.5})$$

Taking into account that the wave field inside the body is $\exp(j\omega t - jpx - jq_{l,t}y)$, $y > 0$ for instance, the x -component of Poynting vector is $\Pi_1 = .5\text{Re} \{ \mathbf{T}\dot{\mathbf{u}}^* \}$, that is

$$\begin{aligned} \Pi_1(y) &= -\frac{1}{2}\text{Re} \{ k_t^{-2} [F_l \ F_t] \mathbf{X} [F_l^* \ F_t^*]^T \} \\ \mathbf{X} &= \mathbf{E} \begin{bmatrix} 2q_l^2 - k_t^2 & -2pq_l \\ 2pq_t & 2q_t^2 - k_t^2 \end{bmatrix} \begin{bmatrix} p^* & -q_t^* \\ q_l^* & p^* \end{bmatrix} \mathbf{E}^*, \end{aligned} \quad (\text{C.6})$$

where $\mathbf{E} = \text{diag}(e^{-jq_l y}, e^{-jq_t y})$.

For real $q_{l,t}$ this yields the y -averaged value analogous to (C.3)

$$\Pi_1 = \text{Re} \{ p|F_l|^2 + p|F_t|^2 \} / 2, \quad (\text{C.7})$$

but in our analysis, where both p and q 's are complex, the wave field decays in depth of the body and we need the total power carried in the domain $y \in (0, \infty)$. This requires integration of Eq. (C.6) term by term

$$\Pi_x = \int_0^\infty \Pi_1(y) dy \quad (\text{C.8})$$

(the resulting formula is too complex to be presented here). The above relations can be applied to any Bloch component of an interface wave under substitution $p = -r_c + nK$.

Appendix D: Low Bloch components

The boundary value problem for interface crack waves is closed in the homogeneous system (A.1), (A.3) taken with $\mathbf{T}^I = 0$, or equivalent system (B.3) taken with $\dot{\mathbf{u}} = 0$; its solution is then eventually applied in other equations to obtain corresponding wave field components, particularly \mathbf{T} , that may characterize the wave amplitude. For given \mathbf{T} , we use Eqs. (A.5) in place of (A.3) to evaluate \mathbf{t}_m and then the other wave field components, particularly the lower Bloch components of interface stress, $\mathbf{T}_{0,\pm 1}$ from Eq. (A.4) at $n = 0, \pm 1$. In the case of interface waves (no incident bulk wave, $\mathbf{T}^I = 0$), these are equal stresses on both sides of the contacting halfspaces that can be used in Eqs. (C.3), (C.8) in order to evaluate the corresponding power flux.

The most important are powers carried along the interface by ± 1 Bloch components: $\Pi^{(\pm 1)}$, and in depth of the body by 0-th component, Π_y . (The ± 1 components can carry comparable powers in opposite directions; this is a typical phenomenon in periodic systems [8]; the ratio $\gamma^2 = -\Pi^{(-1)}/\Pi^{(1)}$ describes the standing wave coefficient). These powers determine the total power carried by an interface wave along the interface, $\Pi^c = \Pi^{(1)} + \Pi^{(-1)}$ and the power shed into bulk due to the leakage phenomenon, Π_y . Both directly evaluated crack wave power and the total shed power agree perfectly in computations. One may thus conclude that the other Bloch components contribute negligibly to the energy transport in the system; this is also evident from Eq.(C.8) applied for wave components having large $p = -r_c + K$.

Appendix E: Maximum efficiency

THEOREM. $2\eta_1 \leq 1/2$ results from the system symmetry.

PROOF. In certain units, the interface wave power is $|a\mathbf{T}|^2$, while the incident power is $|\mathbf{T}^I|^2/Z_c$, and reflected and transmitted powers are $|\mathbf{T} - \mathbf{T}^I|^2/Z_c$ and $|\mathbf{T}|^2/Z_s$, respectively, see Eqs. (3) of [1] for stress in the upper and lower elastic halfspaces. We apply index c for the acoustic impedance Z of a comb, and s of a sample.

The energy conservation law states that

$$2|a\mathbf{T}|^2 + |\mathbf{T} - \mathbf{T}^I|^2/Z_c + |\mathbf{T}|^2/Z_s = |\mathbf{T}^I|^2/Z_c, \tag{E.1}$$

resulting in

$$|\mathbf{T}| = |\mathbf{T}^I| \frac{\cos \theta / Z_c}{a^2 + \alpha}, \quad \alpha = (Z_c^{-1} + Z_s^{-1})/2, \tag{E.2}$$

where θ is a possible phase shift between \mathbf{T} and \mathbf{T}^I . Substituted into expression for the interface wave power, this yields

$$\Pi^c / P^I = \frac{2}{Z_c} \frac{a^2 \cos^2 \theta}{(a^2 + \alpha)^2}, \tag{E.3}$$

which ratio has maximum at $a^2 = \alpha$, thus

$$2\Pi^c / P^I = \frac{\cos^2 \theta}{1 + Z_c/Z_s} \tag{E.4}$$

that is less than a half for the considered case of $Z_c = Z_s$. Only 50% of the incident power can be transformed into crack waves in both directions.

Making a digression, let's consider a bulk wave beam scattering on a solid surface with periodic grooves on it; this arrangement was proposed for generation of surface waves [8]. There is not transmitted bulk wave, thus the last term on the left hand side of (E.1) must be neglected, and we easily obtain that up to 100% of the incident power can be transformed into Rayleigh waves in this arrangement.

Appendix F: Edge scattering

Here we apply an approximation [9] to the planar harmonic Green's function of arbitrary elastic halfspace assuming that the normal stress vanishes at the body surface. For harmonic waves $\exp(j\omega t - jpx)$ on the surface, we have

$$u = \frac{1}{\sqrt{p^2}} \frac{\sqrt{p^2 - k_t^2}}{\sqrt{p^2 - k_t^2} - \alpha \sqrt{p^2}} T, \tag{F.1}$$

where $u = u_1$ and $T = T_{12}$, in certain units that are not important here. The approximation is valid in vicinity of k_t , but we apply it in the whole domain of spectral variable p ; this yields the simplest model of elastic halfspace supporting only shear bulk wave mode which is cut-off at $|p| = k_t$. The halfspace supports also a Rayleigh wave (for $T = 0$) having wave number $k_R > k_t$ at zero of denominator (F.1).

To model crack interface waves having wave number $k_c > k_t$ at another boundary conditions, we put an elastic layer on the halfspace described by $\Delta T = eu\sqrt{p^2}$ where ΔT is the stress difference on both sides of the layer (although it is considered infinitesimally thin). The stress on the top of the system is

$$T' = T + \frac{e}{\sqrt{p^2}}u = (1 + e)\frac{\sqrt{p^2 - k_t^2} - \beta\sqrt{p^2}}{\sqrt{p^2 - k_t^2} - \alpha\sqrt{p^2}}T, \quad (\text{F.2})$$

$\beta = \alpha/(1 + e)$. There is another surface wave for $T' = 0$,

$$k_R = k_t/\sqrt{1 - \alpha^2}, \quad k_c = k_t/\sqrt{1 - \beta^2}. \quad (\text{F.3})$$

The layer is semiinfinite, residing at $x < 0$, and its edge correspond to the edge of comb transducer; the rest of the body surface, $x > 0$, is free where a Rayleigh wave can propagate. We are going to consider a scattering problem with incident "interface" wave $\exp(j\omega t - jk_c x)$, $x < 0$, propagating from $-\infty$ towards the edge at $x = 0$ where it scatters producing the reflected interface wave $\exp(j\omega t + jk_c x)$, $x < 0$, and a transmitted Rayleigh wave $\exp(j\omega t - jk_R x)$, $x > 0$, and also the scattered bulk waves.

It is convenient to introduce certain Rayleigh ($x > 0$) and interface ($x < 0$) modal amplitudes F^+ and F^- , respectively, related to the mode powers by $.5|F^\pm|^2$. Equation (F.2) can be transformed into

$$F^- = \frac{1}{\sqrt{\xi}}\sqrt{\frac{\alpha}{\beta}\frac{1 - \beta^2}{1 - \alpha^2}}\frac{\sqrt{p^2 - k_t^2} - \beta\sqrt{p^2}}{\sqrt{p^2 - k_t^2} - \alpha\sqrt{p^2}}F^+, \quad (\text{F.4})$$

that is convenient for Jones' formulation of the Wiener-Hopf problem [6] where $1/(p - k_c)$ describes the incident wave,

$$F^- + \frac{1}{p - k_c} = A\frac{p^2 - k_R^2}{p^2 - k_c^2}\frac{G_\beta(p)}{G_\alpha(p)}F^+, \quad (\text{F.5})$$

$$G_a(p) = \frac{1}{1 + a}\left(1 + \frac{a\sqrt{p^2}}{\sqrt{p^2 - k_t^2}}\right) \rightarrow 1 \quad \text{at } |p| \rightarrow \infty,$$

which $G_a(r)$, $a = \alpha, \beta$, can be easily factorized into $G_a^+G_a^-$, a product of functions regular in either upper or lower complex halfplanes of p , $A^2 = [(1 - \alpha)/(1 + \alpha)][(1 + \beta)/(1 - \beta)]\alpha/\beta$.

The standard separation of functions regular in different complex halfplanes yields

$$F^- = \left[\frac{p + k_R}{p + k_c} \frac{G_\beta^-(p)}{G_\alpha^-(p)} \frac{2k_c}{k_c + k_R} \frac{G_\alpha^-(k_c)}{G_\beta^-(k_c)} - 1 \right] \frac{1}{p - k_c}, \quad (\text{F.6})$$

$$F^+ = \frac{1}{A} \frac{2k_c}{k_c + k_R} \frac{G_\alpha^-(k_c)}{G_\beta^-(k_c)} \frac{G_\alpha^+(p)}{G_\beta^+(p)} \frac{1}{p - k_R}.$$

An applied inverse Fourier transform would yield the solution, but we are interested only in the modal amplitudes which are determined by corresponding residua at poles $-k_c$ and k_R .

Both $k_{c,R} > k_t$, and this simplifies evaluation of the required factors of $G_a(p)$, $p = \pm k_{c,R}$

$$G_a^+(p) = \frac{j\sqrt{k_t}}{\sqrt{|p| - k_t}} \exp \left\{ \frac{a}{\pi} \int_0^{\pi/2} \frac{\ln(|p/k_t - \sin \eta|)}{\cos^2 \eta + a^2 \sin^2 \eta} d\eta \right\}. \quad (\text{F.7})$$

It is easy to check that for both $k_{c,R}$ sufficiently larger from k_t ,

$$F^- \approx \frac{k_R - k_c}{k_R + k_c}, \quad F^+ \approx \frac{2\sqrt{k_c k_R}}{k_R + k_c}, \quad (\text{F.8})$$

which power combined, approximately equals the incident power, and thus the scattering into bulk waves is weak. But for k_c close to k_t , both amplitudes of transmitted and reflected modes can be much smaller and large part of the incident power goes into bulk waves.

References

- [1] E.J. DANICKI, *Resonant phenomena in bulk wave scattering by in-plane periodic cracks*, J. Acoust. Soc. Am., **105**, 84–92 (1999).
- [2] E.J. DANICKI, *Periodic crack model of comb transducers: excitation of interface waves*, Arch. Acoust., **25**, 213–227 (2000).
- [3] S. HIROSE and J.D. ACHENBACH, *Higher harmonics in the far field due to dynamics crack-face contacting*, J. Acoust. Soc. Am., **93**, 142–147 (1993).
- [4] D.C. HURLEY, *Measurements of surface-wave harmonic generation in nonpiezoelectric materials*, J. Acoust. Soc. Am., **103**, 2923(A) (1998).
- [5] E.J. DANICKI, *Generation and Bragg reflection of surface acoustic waves in nearly periodic system of elastic metal strips on piezoelectric half-space*, J. Acoust. Soc. Am., **93**, 116–131 (1993); and further relations in: *Spectral theory for IDTs*, 1994 IEEE Ultras. Symp. Proc., 213–222 (1994).
- [6] R. MITTRA and S.W. LEE, *Analytical techniques in the theory of guided waves*, Ch. 3, Macmillan, New York 1971.
- [7] R.E. COLLIN, *Field theory of guided waves*, Ch. 9, McGraw-Hill, New York 1960.
- [8] R.F. HUMPHRYES and E.A. ASH, *Acoustic bulk-surface wave transducer*, Electr. Lett., **5**, 175–176 (1969).
- [9] E.J. DANICKI, *An approximation to the planar harmonic Green's function at branch points in wave-number domain*, J. Acoust. Soc. Am., **104**, 651–663 (1998).